ACS APPLIED MATERIALS & INTERFACES

Research Article

www.acsami.org

Modulation of Pore Sizes of Titanium Dioxide Photocatalysts by a Facile Template Free Hydrothermal Synthesis Method: Implications for Photocatalytic Degradation of Rhodamine B

Shivatharsiny Rasalingam, Chia-Ming Wu, and Ranjit T. Koodali*

Department of Chemistry, University of South Dakota, Vermillion, South Dakota 57069, United States

Supporting Information

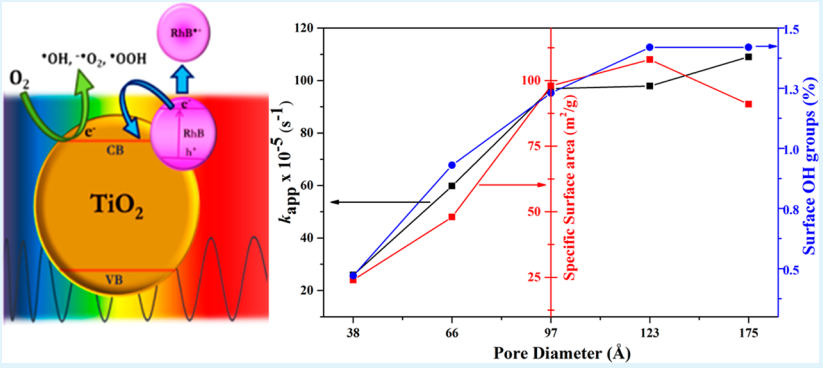

ABSTRACT: Mesoporous TiO_2 photocatalysts were prepared in ethanol media by using relatively green, template free sol−gel technique. A mild hydrothermal treatment procedure was employed to tune the pore sizes of the materials. Comprehensive techniques that include powder X-ray diffraction, diffuse reflectance spectroscopy, specific surface area analysis, electron microscopy, FT-IR, TGA, and ζ-potential measurements were used to characterize the titania materials. Porosity (pore size and pore volume) of the materials were found to be key factors for the variation in the rate of photocatalytic degradation of rhodamine B; in addition to specific surface area, and surface hydroxyl groups. An increase in porosity permits effective transport of the dye molecules resulting in an increase in the rate of the degradation in materials having larger pores. A detailed electrospray ionization-mass spectrometric (ESI-MS) study was carried out for selected materials to identify photodegraded intermediates and products formed during the degradation of rhodamine B. In addition, experiments were also carried out to understand the role of reactive oxygen species (ROS). In summary, this work provides a simple way to tune pore sizes without the use of any template and an insight into the influence of pore size for the photocatalytic degradation of rhodamine B.

KEYWORDS: *photocatalysis, hydrothermal treatment, pore size, degradation, rhodamine B*

INTRODUCTION

Environmental pollution is of great concern to Earth's sustainability mainly due to waste mismanagement in industrial processes and the effects of inadvertent development. In particular, organic pollutants that include dyes,[1] substituted phenols,[2,3] and agricultural wastes[4] are released into the environment and can be transported over long distances in the atmosphere, water, and land. Most of these pollutants have characteristic features, such as low water solubility, high lipid solubility, semivolatility, and high molecular masses, that enable their prevalence in air, land, and water sources for a long time period. For example, dyes, which contain nitrogen groups (Azo-dyes), can be naturally reduced under anaerobic conditions and form very toxic products. Hence, numerous techniques, such as membrane filtration,[5] coagulation and flocculation,[6] electrochemical oxidation,[7] adsorption,[8−10] biological treatment,[6,11] and advanced oxidation processes (AOP)[12−19] have been established for water purification.[20,21] Even though, these techniques have certain practical applications, some of them are nondestructive and show low efficiencies. Adsorption is supposed as a promising water treatment method for the industrial applications owing to its ease of operation and cost-effectiveness. However, adsorption only removes pollutants from the aqueous phase and transfers them onto a solid matrix.[22]

AOP, which involves highly reactive oxygen species (ROS), such as $^{\bullet}OH$, $O_2^{\bullet-}$, and $^{\bullet}OOH$, have emerged as an efficient method for the mineralization of organic pollutants.[23] Among these species, hydroxyl radicals ($^{\bullet}OH$) are very reactive[24,25] and extremely unstable because of its high oxidation potential (2.80 V). Heterogeneous photocatalytic reactions have garnered

Received: December 17, 2014
Accepted: January 29, 2015
Published: January 29, 2015

DOI: 10.1021/am508883f
ACS Appl. Mater. Interfaces 2015, 7, 4368−4380

extensive attention because of the effective removal of hazardous wastes and toxic chemicals.[4,26−28]

Titania based materials have been extensively used as photocatalysts for water purification.[17,29] In particular, the application of these oxides and mixed oxide materials toward degradation of dyes that include methylene blue,[30−32] methyl orange,[13,33] rhodamine B (RhB),[34−40] rhodamine 6G, eosin Y,[29] etc., and phenolic compounds, for example, phenol,[41,42] chlorophenol,[2,43,44] and nitrophenol,[45−47] are reported in literature. These reports have shown some correlation between the rate of degradation and the structural properties of the photocatalysts, including crystallinity[48] and specific surface area.[40,49]

The degradation of bulky molecules and dyes is effective in materials that possess favorable textural properties, such as large pore sizes and pore volumes. This is because materials that have large pore volumes can accommodate or adsorb relatively larger amounts of dyes and large pore sized materials provide efficient transport pathways for molecular trafficking. Surprisingly, the role of pore sizes of photocatalysts and their effect on degradation of dyes have not been systematically examined. Attempts have been made to modulate the porosities of photocatalytic materials, but the reported works utilize cosolvents,[50] surfactants,[51] structure modifying agents, such as urea,[52,53] polymers, and use different calcination temperatures,[54] or calcination time[55] to modify the porous nature of the catalysts. Hence, the findings in previous reports related to the degradation of organics are lacking in one or more of the following: (i) a facile greener, template or structure directing agent free, synthesis method to tune the textural properties, such as specific surface area, pore size, and pore volume, of mesoporous TiO_2 materials, (ii) a comprehensive physicochemical characterization of the photocatalysts (TiO_2), (iii) the effect of pore size on the rate of degradation, (iv) a comprehensive study of the identification of the photodegraded products for visible light induced degradation of RhB from ESI-MS studies, (v) a detailed mechanistic study to understand the role of ROS such as hydroxyl radicals ($^{\bullet}OH$), in the dye degradation process, and (vi) a better understanding of the structural property and the photocatalytic activity relationship. Thus, this work fills a gap in literature and offers a structure−activity relationship for the degradation of a model organic pollutant and provides guidance toward the development of efficient photocatalysts for environmental remediation.

In summary, this article demonstrates a simple, environment friendly, synthetic procedure for the preparation of TiO_2 photocatalysts through a sol−gel method in the presence of a polar solvent, ethanol. Ethanol is more industrially friendly, less toxic, and is considered as a green solvent.[56,57] Furthermore, a template free hydrothermal preparation method has been developed by simply changing the hydrothermal treatment temperature and this leads to the modulation of the structural properties of the materials. The photocatalytic degradation of RhB was examined in this study and the results suggest that the pore size of the materials is critical for degradation. We believe that these findings will offer better guidance to researchers involved in the discipline of photocatalysis and environmental remediation.

EXPERIMENTAL SECTION

Materials. Commercially available titanium isopropoxide (Ti(^{i}OPr)$_4$) (Acros, 98+%), anhydrous ethanol (Pharmco-AAPER, ACS/USP grade), and conc. HNO_3 were used as received to prepare the TiO_2 photocatalysts. RhB (Alfa Aesar) was used as is. Deionized water (resistivity > 18.2 Ω.cm) was used to prepare the solution mixtures. Terephthalic acid (TPA, Acros, 98%) and isopropyl alcohol (Fisher scientific) were used as received. Optima grade water was used for the ESI-MS studies.

Synthesis of Ti-HTS Materials. The photocatalysts were prepared by adding 32.5 mL of ethanol and 0.30 mL of conc. HNO_3 under stirring at 300 rpm followed by the dropwise addition of (Ti(^{i}OPr)$_4$) (6.6 mL). Finally, 3.0 mL of water was added dropwise with rapid stirring. Stirring was stopped when a gel was formed. It was then kept for hydrothermal treatment in an autoclave at different temperatures, 40°, 90°, 150°, 210°, and 240 °C for overnight. After hydrothermal synthesis, the precipitate obtained was filtered, washed, and oven-dried at ∼80 °C for 9 h. The materials were ground and calcined by heating in static air at 500 °C for 6 h at a heating rate of 3 °C/min. The resulting materials are labeled as Ti-HTS-40, Ti-HTS-90, Ti-HTS-150, Ti-HTS-210, and Ti-HTS-240, where HTS refers to hydrothermal synthesis and the number refers to the hydrothermal temperature.

Characterization. The calcined materials were characterized by using different techniques. The Powder X-ray diffraction (P-XRD) patterns were recorded on a Rigaku Ultima IV instrument with Cu Kα radiation (λ = 1.5408 Å) at ambient temperature, under the following operating conditions; accelerating voltage of 40 kV; emission current of 44 mA; scanned range (2θ) between 20 and 80° with a step size of 0.02° and a scan speed of 1°/min. By applying the Debye−Scherrer equation to the peaks at 2θ = 25.4, 48.3°, and 62.9° the crystallite sizes of the titania phase in the mixed oxide materials were determined. The diffraction patterns were analyzed using PDXL software provided by Rigaku. Raman spectra were collected using a Horiba Jobin Yvon LabRam ARAMIS spectrophotometer with an internal He−Ne (532 nm) excitation laser. The unfiltered beam of scattered laser radiation was focused onto the sample through a microscope objective (×50) for an acquisition time of 10 s and repetition of 10×. The radiation was then dispersed by a 1800 line/mm grating onto the CCD detector. The diffuse reflectance spectra (DRS) were obtained in the range between 200 and 700 nm using a Carry 100 Bio UV−vis spectrophotometer equipped with a Harrick DR praying mantis accessory. Nitrogen physisorption studies were measured using the Quantachrome Nova2200e specific surface area analyzer. The TiO_2 materials were dried overnight at 70 °C followed by extensive degassing at 110 °C. These degassing conditions have emerged sufficient since our materials do not retain excess amounts of solvent as confirmed by thermogravimetric analysis (TGA). The adsorption−desorption isotherms were obtained at 77 K using N_2 as the carrier gas. The specific surface areas of the TiO_2 materials were calculated using the Brunauer−Emmett−Teller (BET) equation within the relative pressure P/P_0 range of 0.05−0.30. The pore volume was attained from the nitrogen amount adsorbed at the highest relative pressure $P/P_0 \approx$ 0.99. The pore size distribution was determined by applying the Barrett−Joyner−Halenda (BJH) equation to the desorption isotherm. Fourier Transform-Infrared (FT-IR) spectra were obtained between 400 and 4000 cm^{-1} on a Bruker-Alpha FT-IR instrument model ALPHA equipped with ATR platinum diamond crystal plates, by taking 24 scans at a resolution of 4 cm^{-1}. The surface charge of the TiO_2 materials was recorded by auto titration using a zetasizer analyzer and by adjusting the pH of TiO_2-electrolyte (KNO_3 in DI water) suspension. A Malvern NanoZS-90 zetasizer was used to measure the zeta potential (ζ) of the TiO_2 materials. Deionized water was used as the diluent. Test samples were prepared with the molarity of 1 mg mL^{-1} by dispersing known amounts of the samples in aqueous 0.01 M KNO_3 solution. The pH was controlled by addition of 0.1 M KOH and/or HNO_3. The synthesized TiO_2 materials were further characterized by transmission electron microscopy (TEM, FEI Tecnai G^2) and scanning electron microcopy (SEM, FEI Quanta 450).

Photocatalytic Experiments. The photocatalytic experiments were performed by the following procedure. Twenty-five milligrams of the photocatalyst was dispersed in 50 mL of RhB 2×10^{-5} M (initial pH ∼ 5−6) solution in a quartz cylindrical jacket reactor, and stirred in the dark at 300 rpm for 30 min to establish the adsorption−desorption equilibrium. Then, visible light was supplied by a Xenon arc lamp

DOI: 10.1021/am508883f
ACS Appl. Mater. Interfaces 2015, 7, 4368−4380

(Newport 1000 W) through a Pyrex glass filter (cut off 420 nm). The light intensity on the photocatalytic reactor was ~98 mW cm^{-2}. The reaction temperature was maintained at 25 ± 2 °C by channeling water in between the walls of the reactor throughout the course of the experiment. Five mL of the reaction mixture was withdrawn at 30 min intervals, then centrifuged at 3200 rpm for 20 min and the clear supernatant was analyzed using UV−vis spectroscopy as discussed later.

Additional experiments were carried out under N_2 flow (absence of oxygen) and with isopropyl alcohol (IPA) to examine the roles of $O_2^{\bullet-}$, and $^{\bullet}OH$ radicals, respectively. To detect the amount of $^{\bullet}OH$ formed on irradiated TiO_2 surfaces, terephthalic acid (TPA) was used as a chemical trap for the $^{\bullet}OH$ radicals. It is well-known that $^{\bullet}OH$ radicals rapidly react with TPA to produce highly fluorescent 2-hydroxyterephthalic acid (2-HTPA). In a typical procedure, 25 mg of photocatalyst were added to 50 mL of 5×10^{-4} M TPA solution in 2×10^{-3} M NaOH and stirred well to obtain homogeneous suspension prior to irradiation. Three milliliters aliquots were drawn every 20 min, filtered through a 0.45 μm Millipore filter membrane, and the clear solution was analyzed using Fluoromax-4 (JY Horiba) fluorometer. The fluorescence emission intensity of the 2-hydroxyterephthalic acid was recorded at 425 nm after excitation at 315 nm. The intensity of the peak at 425 nm is estimated to be proportional to the amount of $^{\bullet}OH$ formed.

Analytical Techniques. The remnant concentration of the dye solution after the photocatalytic reaction was estimated by UV−vis spectrophotometric method. The absorbance was recorded by following the peak at 554 nm, which corresponds to the absorption maximum of RhB. Quantification of the RhB concentration at different time intervals was completed by using a calibration plot of RhB in the concentration range between 1×10^{-6} and 1×10^{-4} M.

A Varian 500-MS Ion Trap Mass Spectrometer was used for the identification of the fragmented dye compounds that are formed during the photocatalytic degradation. Ionization was completed by electrospray ionization (ESI) source in positive mode to separate the fragments on the basis of their mass to charge ratio with 1:1 volume ratio of optima grade methanol and dye solution mixture. The operating parameters used for MS study are summarized in the Supporting Information (Table S1). The obtained catalyst-dye suspensions at different time intervals were centrifuged and then filtered over 0.45 μm filter. The filtrate was infused into the mass spectrometer for analysis. Owing to the unavailability of standards, the quantitative determination of fragmented products could not be performed.

RESULTS AND DISCUSSION

Physicochemical Characterization. The phase composition of the samples were analyzed using P-XRD analysis and Figure 1 represents the XRD plots of Ti-HTS-40, Ti-HTS-90, Ti-HTS-150, Ti-HTS-210, and Ti-HTS-240 materials prepared at different hydrothermal treatment temperatures of 40°, 90°, 150°, 210°, and 240 °C, respectively. The results suggest that the crystallinity of Ti-HTS-40, Ti-HTS-90, and Ti-HTS-150 are similar, whereas an increase in temperature to 210 and 240 °C results in a small but notable decrease in intensity. All the samples exhibit peaks at 2θ = 25.4°, 37.9°, 48.2°, 54.1°, 55.1°, 62.6°, 68.9°, 70.4°, and 75.1° that correspond to d-spacings of d_{101}, d_{004}, d_{200}, d_{105}, d_{211}, d_{204}, d_{116}, d_{220}, and d_{215}, respectively, which are typically attributed to the anatase phase. Notably, the sample Ti-HTS-90 shows a small peak at 2θ = 27.4° that is due to the rutile phase of TiO_2. However, the percentage of rutile phase could not be clearly determined since it was very low in comparison to the anatase phase. The exact reasons as to why rutile is formed only for this material is still unclear to us. In addition, Raman spectroscopic analysis (discussed below) suggests that the absence of rutile in Ti-HTS-90.

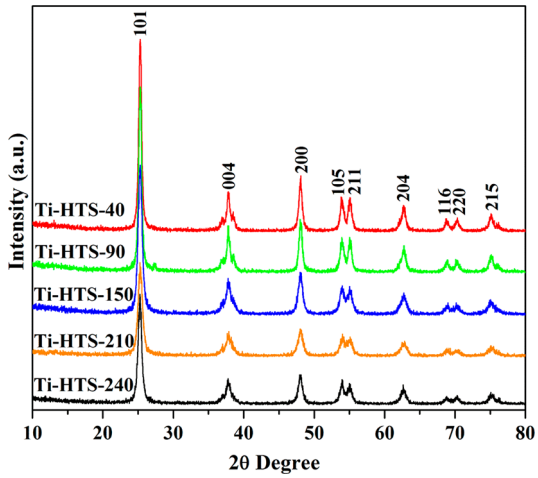

Figure 1. Powder X-ray diffraction patterns of TiO_2 materials prepared at hydrothermal temperatures of 40, 90, 150, 210, and 240 °C.

Raman studies further supported the presence of predominantly anatase phase and the crystalline nature of the TiO_2 materials as illustrated in Supporting Information Figure S1. All the TiO_2 materials exhibit peaks at 638, 510, and 391 cm^{-1} corresponding to $E_{g(3)}$, $B_{1g(2)}$, and $B_{1g(1)}$ symmetry modes, respectively. A peak at 197 cm^{-1} may be due to the $E_{g(1)}$ symmetric modes. Thus, powder XRD and Raman studies of TiO_2 results indicate high crystallinity of titania materials and the presence of primarily anatase phase.

The band gap energies for the TiO_2 materials, corresponding to the absorption spectra of the solid samples (Figure 2A), were estimated by using the Tauc plot (Figure 2B), which were transformed via the Kubelka−Munk function, $[F(R_\infty)E]^n$ versus E, when n = 0.5, for a direct allowed transition. The estimates derived from the Tauc plots in Figure 2B suggest that the bandgaps of Ti-HTS-40 (3.10 eV), Ti-HTS-90 (3.06 eV), Ti-HTS-150 (3.20 eV), Ti-HTS-210 (3.16 eV), and Ti-HTS-240 (3.18 eV) lie in a narrow range and are in good agreement with the anatase phase of TiO_2 (3.2 eV).

The nitrogen isotherms of TiO_2 materials prepared at different hydrothermal treatment temperatures are depicted in Figure 3A. All the materials exhibit a characteristic type IV isotherm of mesoporous materials. Monolayer adsorption was achieved in the initial part of the isotherm and a multilayer adsorption and subsequent capillary condensation occurs with an increase in the relative pressure. Typically, the filling and emptying of pores takes place at separate relative pressure values resulting in hysteresis, which is a reflection of the degree of pore connectivity in these materials, and all TiO_2 materials may be classified as belonging to the H2 type of hysteresis loop. Figure 3B illustrates the pore size distribution of the TiO_2 materials. The catalyst Ti-HTS-40 exhibited pores predominantly centered at 38 Å. An increase in hydrothermal temperature results in an increase in pore diameter up to 175 Å and the results are summarized in Table 1.

It has been reported that the pore sizes of the materials can be tuned by using surfactants,[51] structure modifying agents (i.e., urea or urea-glycol mixture),[52,53] polymeric swelling agents,[58] and also by changing the calcination temperature and time.[54] In this study, the pore sizes of the materials could be tuned by simply adjusting the hydrothermal treatment temperature. To the best of our knowledge, this is the first report modulating the pore size of aperiodic mesoporous TiO_2 materials by simply

DOI: 10.1021/am508883f
ACS Appl. Mater. Interfaces 2015, 7, 4368−4380

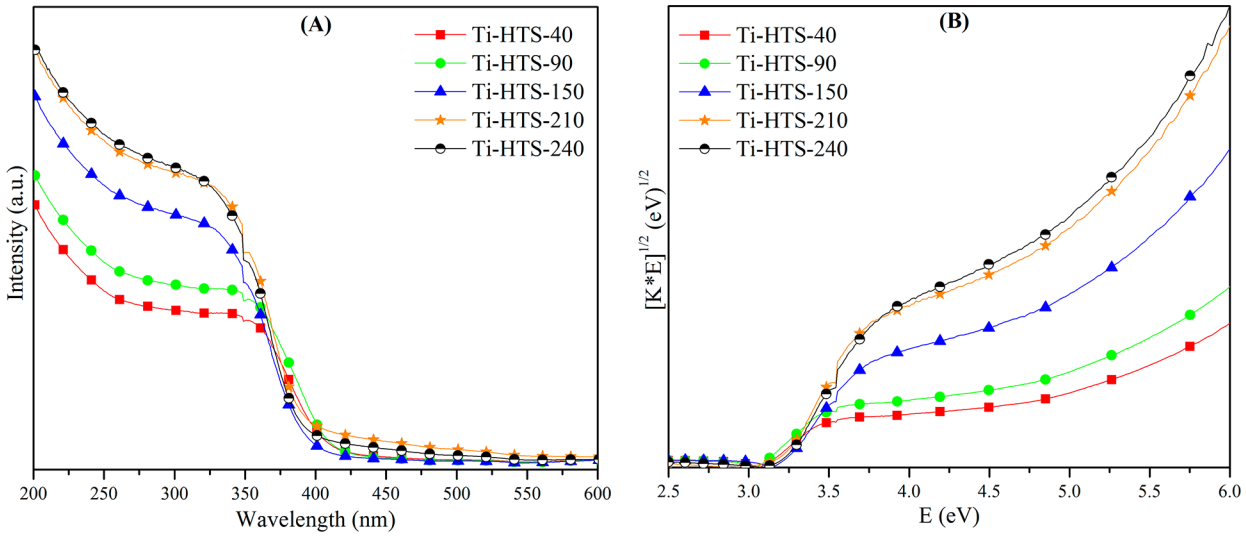

Figure 2. (A) Diffuse reflectance spectra and (B) Tauc plots of TiO_2 materials prepared at hydrothermal temperatures of 40, 90, 150, 210, and 240 °C.

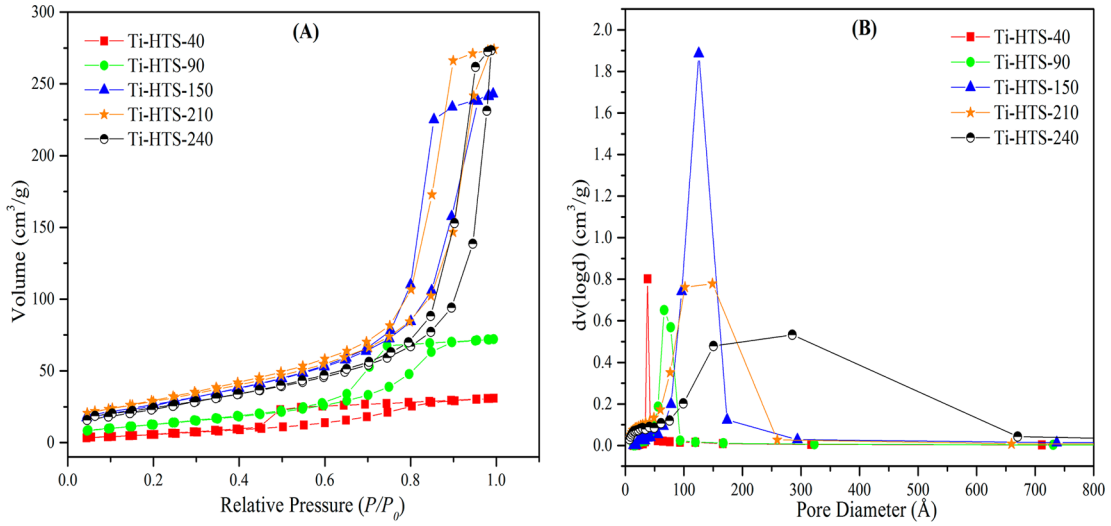

Figure 3. (A) N_2 physisorption isotherms and (B) BJH pore size distribution plots of TiO_2 materials prepared at different hydrothermal temperatures of 40, 90, 150, 210, and 240 °C.

Table 1. Textural Properties of Crystalline TiO_2 Materials[a]

sample	SSA (m^2/g)	PV (cm^3/g)	PD (Å)	B_g (eV)	IEP
Ti-HTS-40	24	0.05	38	3.10	8.46
Ti-HTS-90	48	0.11	66	3.06	8.58
Ti-HTS-150	98	0.33	97	3.20	8.87
Ti-HTS-210	108	0.42	123	3.16	8.55
Ti-HTS-240	91	0.42	175	3.18	8.63

[a]Ti-HTS refers to TiO_2 hydrothermal synthesized materials and the numbers denotes the hydrothermal treatment temperature in °C. SSA, PV, and PD refer to specific surface area, pore volume, and BJH pore diameter, respectively. B_g refers to band gap energy, and IEP refers to isoelectric point.

changing the hydrothermal temperature without using any surfactants, structure directing agents, templates or auxiliary chemicals in the synthesis process and under subcritical temperatures.

The variation of the pore size with hydrothermal synthesis temperature can be explained briefly as follows. In sol–gel chemistry, hydrolysis and condensation are two important reactions. These two reactions depend on factors, such as nature of the metal alkoxide and solvent, time, pH, and temperature etc. The factors governing the final morphology, structure, porosity, and particle size distribution of the nanomaterials are dependent on the relative rates of the hydrolysis and condensation reactions, and their subsequent growth and aggregation of the particles. The rates of hydrolysis and condensation of titanium alkoxide are fast and comparable. This is particularly true when the water to alkoxide ratio is greater than the stoichiometric value as is the case in this work. Thus, after addition of water to a mixture of ethanol, titanium isopropoxide, and conc. HNO_3, at room temperature, a gel is formed instantly because of rapid nucleation and growth. This is followed by agglomeration resulting in the formation of primary particles of titania that are amorphous in nature prior to hydrothermal treatment. Use of other alcohols in general leads to a decrease in porosity and hence ethanol was used as the solvent in this study.

DOI: 10.1021/am508883f
ACS Appl. Mater. Interfaces 2015, 7, 4368–4380

The porosity of materials prepared by the sol−gel method is dependent on nature and size of the primary particles formed by hydrolysis and condensation reactions, and the subsequent aggregation and collapse of the gels. All the materials were synthesized and eventually (after hydrothermal treatment) calcined under identical conditions. Hence, the formation of mesoporous structures with variable pore sizes seems to be dependent on the temperature of hydrothermal synthesis. The highest temperature used was 240 °C, because the ionic product of water is maximum in the temperature range of 250−300 °C.

One strategy to tune the porosity of nanomaterials is to regulate the capillary pressure in the pores via control of the liquid−vapor interfacial energy. A reduction in the interfacial energy leads to a reduction in the capillary pressure and this prevents the collapse of the pores. Increasing the hydrothermal synthesis temperature progressively decreases the surface tension (i.e., liquid−vapor interfacial energy) of water and alcohol. This in turn decreases the capillary pressure developed in the pores and thus, the gel is more resistant to collapse as the hydrothermal synthesis temperature increases. Hence the pore sizes and pore volume increases in general with increase in temperature. It is also worth pointing out the trend in pore sizes are similar for the as-synthesized (prior to calcination) titania materials as well indicating that it is the hydrothermal synthesis conditions that regulate the pore sizes. Table 1 lists the textural properties of the materials synthesized in this study.

FT-IR studies show a band near 415 cm^{-1} that is mainly due to Ti−O−Ti bending (Supporting Information Figure S2) and the band at 750 cm^{-1} is due to the Ti−O−Ti stretching vibration. In addition, a band at 929 cm^{-1} is mainly assigned to the Ti−O vibration mode,[59] and the broad band near 3600 cm^{-1} in the two samples Ti-HTS-210 and Ti-HTS-240 are assigned to surface hydroxyl groups. No peaks due to ethanol are seen in FT-IR studies, and this is further validated by TGA studies (Supporting Information Figure S3). TGA results indicate the percentage weight losses in the temperature range of 200−400 °C for Ti-HTS-40, Ti-HTS-90, Ti-HTS-150, Ti-HTS-210, and Ti-HTS-240 to be 0.47, 0.93, 1.23, 1.42, and 1.42, respectively. This can be used to estimate the percentage of surface hydroxyl groups in the materials.[60]

The characteristic morphological features of the photocatalysts were also examined by using electron microscopy. Some fringes were observed, which is an indication of anatase crystallites. A representative TEM image of Ti-HTS-40, which shows fairly high crystallinity in P-XRD analysis, is illustrated in Supporting Information Figure S4. The SEM images of all materials are shown in Supporting Information Figure S5. With changes in the hydrothermal temperature, no distinct changes in the morphologies are observed. All materials show aggregation of primary titania particles into large secondary particles that are several micrometers in dimension.

The surface charge of the samples is summarized in Figure 4 as a function of pH. The isoelectric point (IEP) of TiO_2 materials prepared at different hydrothermal temperatures fall in a narrow range of 8.46−8.87 pH units, which is in proximity with the IEP values for TiO_2 materials reported in previous literature.[61] In regards to the experimental conditions in this study, the pH is around 6. It has been reported that the carboxyl group in RhB can be dissociated at pH values >5. The surface charge of TiO_2 appears to be positive in this range, and, thus, there may be an electrostatic interactions between the surface of TiO_2 and the negatively charged carboxylate ($-COO^-$) groups of RhB.

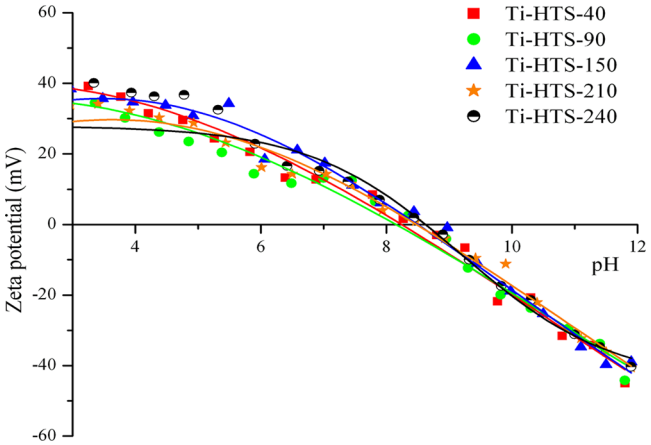

Figure 4. Zeta potential as a function of pH for crystalline TiO_2 materials prepared at different hydrothermal temperatures of 40, 90, 150, 210, and 240 °C.

Photocatalytic Degradation of RhB. Photocatalytic degradation depends on various parameters, such as nature, physicochemical, and optical properties of the semiconductor material, concentration and nature of the organic substrate, intensity of light source, pH of the reaction media, temperature, etc.[62] It has been described elsewhere that RhB is stable under visible light irradiation without photocatalyst,[61] and this was also observed in this study. Without any catalyst, under visible light radiation, the discoloration is small. The remnant concentration of RhB in the presence of visible light irradiation with the photocatalyst was analyzed using UV−vis spectrophotometry (Figure 5). Under visible light irradiation, the RhB molecule absorbs light and get excited to form RhB*. In the next step, an electron is injected into the conduction band of TiO_2. These electrons can react with oxygen molecules to produce ROS, such as $O_2^{\bullet-}$, $^{\bullet}OOH$, and $^{\bullet}OH$.[63] These ROS then attack the dye molecule and destroy the auxochromic groups that lead to the *N*-de-ethylation/de-ethylation of the alkyl amine group and subsequent degradation leading to destruction of the ring structure. Equations 1−7 describe the photocatalytic process involving RhB.

$$RhB + h\upsilon \rightarrow RhB^* \quad (1)$$

$$RhB^* + TiO_2 \rightarrow RhB^{\bullet+} + TiO_2(e^-) \quad (2)$$

$$TiO_2(e^-) + O_2 \rightarrow O_2^{\bullet-} \quad (3)$$

$$O_2^{\bullet-} + H^+ \rightarrow OOH^{\bullet} \quad (4)$$

$$OOH^{\bullet} + O_2^{\bullet-} + H^+ \rightarrow O_2 + H_2O_2 \quad (5)$$

$$H_2O_2 + O_2^{\bullet-} \rightarrow OH^{\bullet} + OH^- + O_2 \quad (6)$$

$$RhB^{\bullet+} + ROS \rightarrow \text{degraded products} \quad (7)$$

N-de-ethylation/de-ethylation can be inferred from the disappearance of the peak at 554 nm. Even though, the disappearance of the peak at 554 nm is not an indication for complete removal of dye molecules, a hypsochromic (blue) shift supports partial *N*-de-ethylation/de-ethylation. This was further evaluated by the ESI-MS analysis and is explained in the next section. In addition, there was a slight blue shift of the

DOI: 10.1021/am508883f
ACS Appl. Mater. Interfaces 2015, 7, 4368−4380

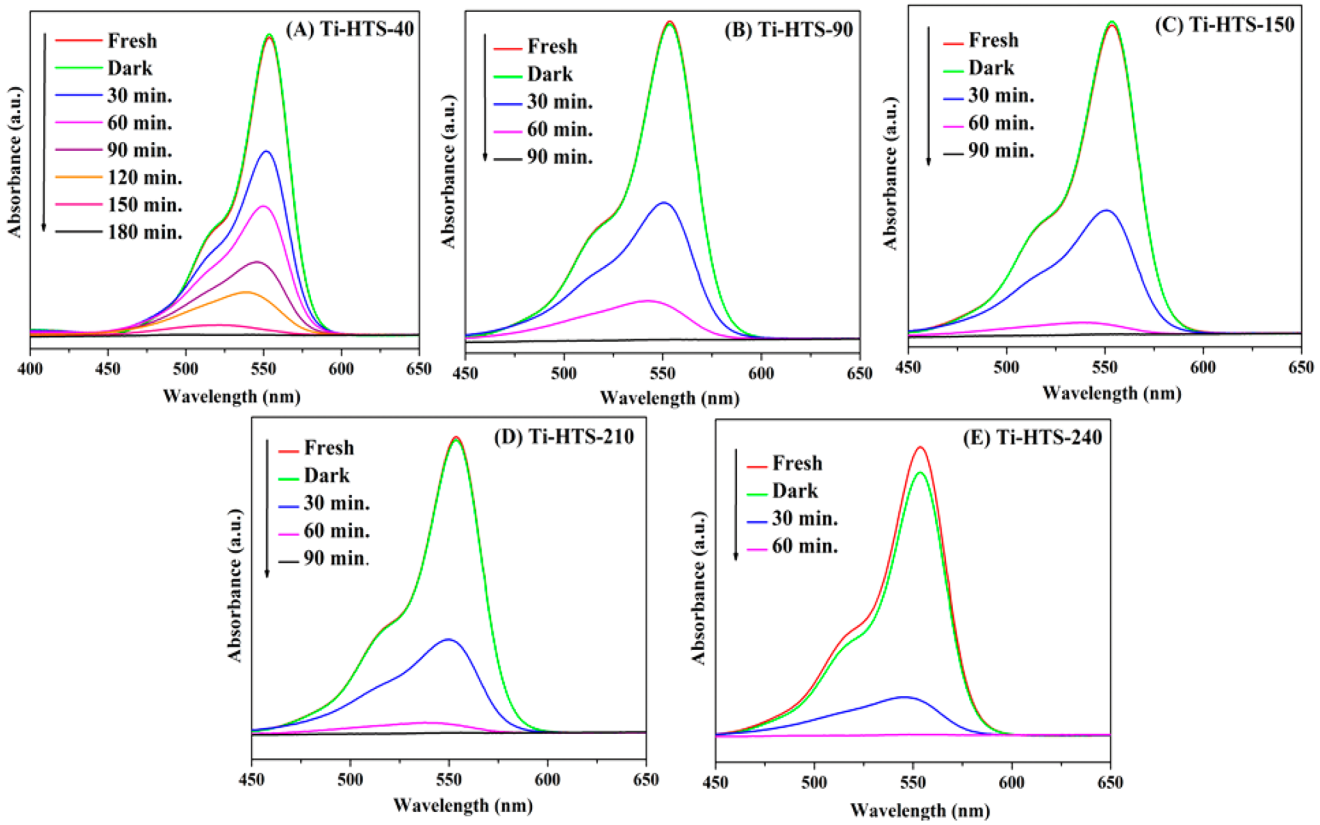

Figure 5. Absorption spectra of RhB dye degraded under visible light irradiation for 6 h using (A) Ti-HTS-40, (B) Ti-HTS-90, (C) Ti-HTS-150, (D) Ti-HTS-210, and (E) Ti-HTS-240 prepared at different hydrothermal temperatures of 40, 90, 150, 210, and 240 °C, respectively.

peak at $\lambda_{max} \approx 258$ nm (corresponding to absorbance from aromatic rings in the dye molecule) which then eventually disappears (Supporting Information Figure S6). This suggests a cleavage of the aromatic structure of the dye molecule.

Figure 6 depicts a plot of C/C_0 vs. time for the degradation of RhB over hydrothermally prepared TiO_2 samples under visible light irradiation, and the values obtained for the apparent rate constant, k_{app} (s^{-1}) are tabulated in Supporting Information Table S2. The TiO_2 materials obey pseudo first-order kinetics, and the apparent rate constant (k_{app}) was calculated from the plot of $\ln(C/C_0)$ vs time. Our present investigation supports our earlier findings.[64] Our results indicate that the amount of RhB adsorbed in the TiO_2 materials was minimal (less than 2%) and thus, the kinetic measurements for these samples were performed under conditions in which only a small fraction of the substrate was adsorbed. Since we are comparing relative trends within a set of samples (that exhibited similar adsorptive properties in the dark), the apparent rate constants (k_{app}) obtained assuming pseudo-first-order kinetics may be used as rough guide to assess the photoactivity among different photocatalysts as recognized by Langford and co-workers.[65]

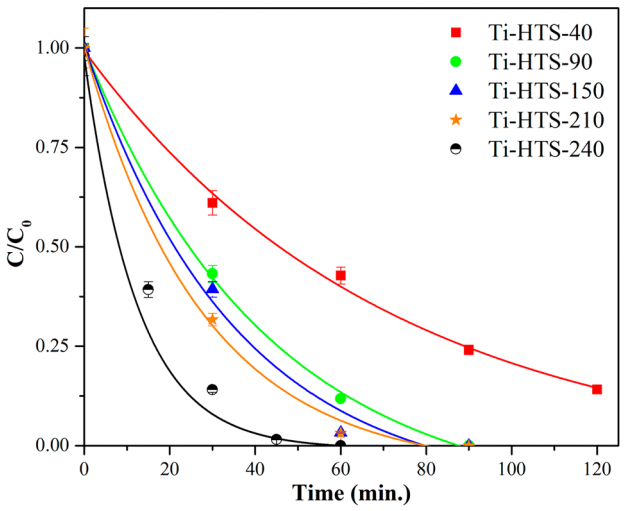

Figure 6. C/C_0 plotted against time for TiO_2 materials under visible light irradiation ($\lambda > 420$ nm).

In photocatalysis, porosity plays an important role in addition to other factors, such as crystallinity, crystallite/particle size, morphology, density of surface hydroxyl groups, specific surface area, etc. The XRD results suggest that the crystallinities of Ti-HTS-40, Ti-HTS-90, and Ti-HTS-150 to be similar and slightly higher than that of Ti-HTS-210 and Ti-HTS-240. The crystallite sizes of these materials vary from 10 to 16 nm and the highest activity was found for Ti-HTS-240, which had a crystallite size of ~12 nm, which is perhaps optimal in this study. The morphology of the five materials do not show any significant differences as indicated in Supporting Information Figure S5. As stated previously, the TGA results (Supporting Information Figure S3) indicate the percentage weight losses in the temperature range of 200−400 °C for Ti-HTS-40, Ti-HTS-90, Ti-HTS-150, Ti-HTS-210, and Ti-HTS-240 to 0.47, 0.93, 1.23, 1.42, and 1.42, respectively. This temperature range is typically used for estimation of surface hydroxyl groups.[60] Thus, the amount of surface hydroxyl groups increase with increase in hydrothermal treatment

DOI: 10.1021/am508883f
ACS Appl. Mater. Interfaces 2015, 7, 4368−4380

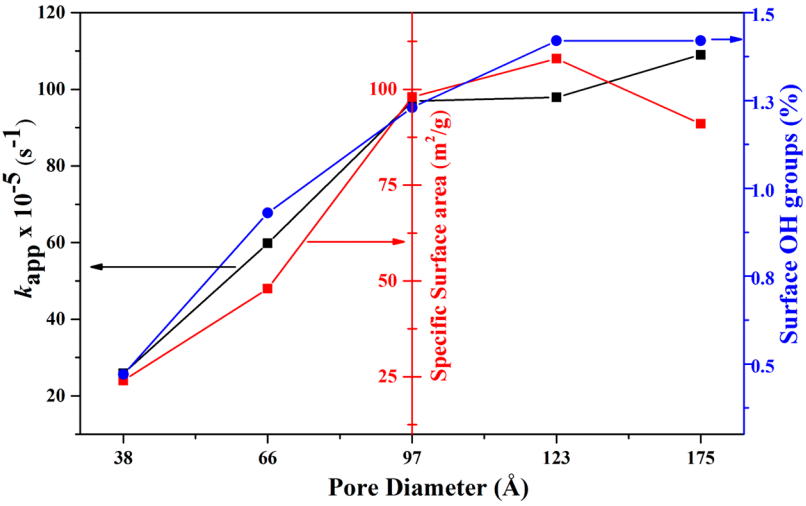

Figure 7. Plot illustrating the correlation between degradation rate constants, specific surface areas, percentage of surface hydroxyl groups, and the pore diameter of TiO_2 materials.

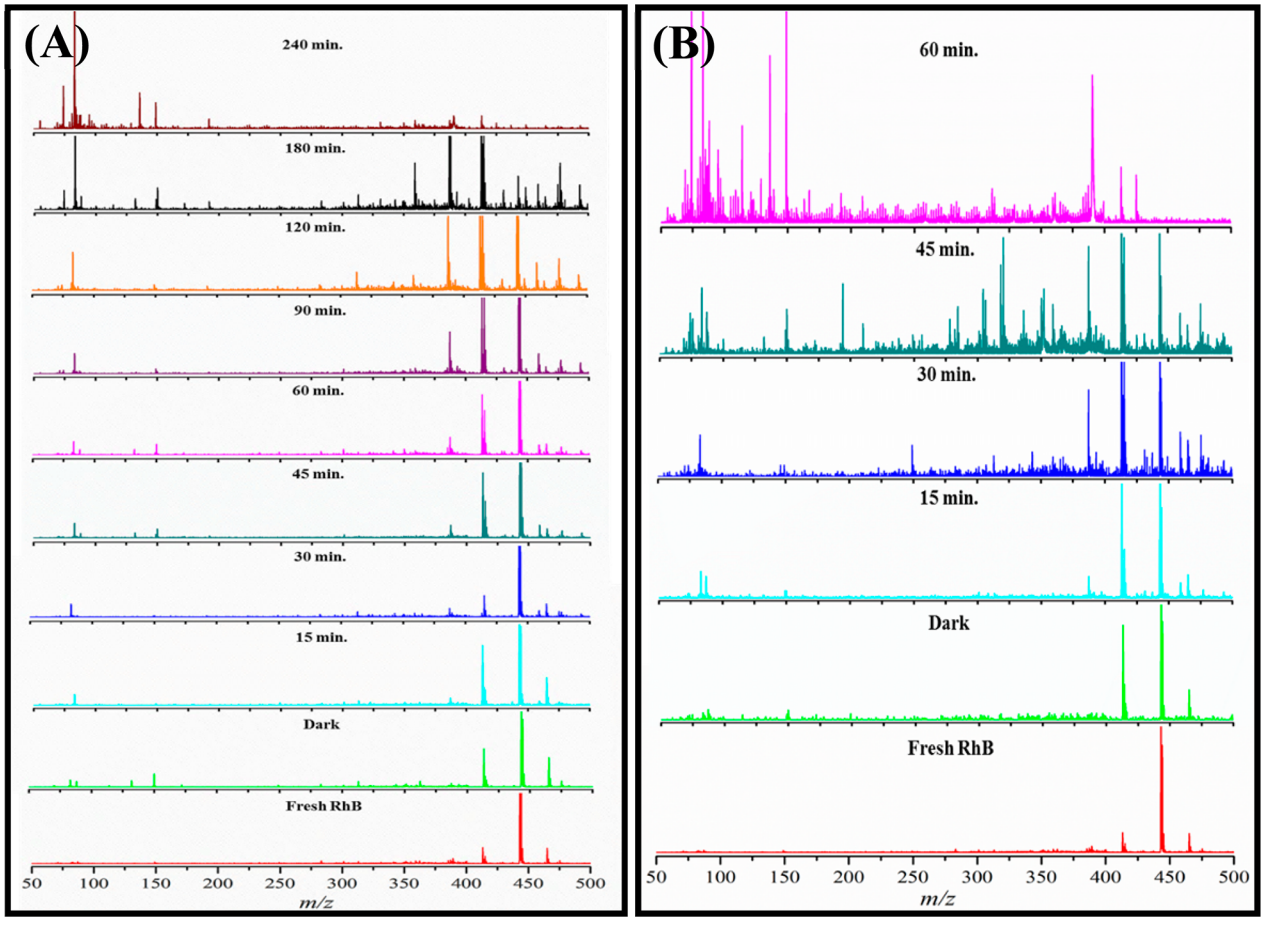

Figure 8. Comprehensive mass spectral data for degraded RhB with time in the presence of (A) Ti-HTS-40 and (B) Ti-HTS-240.

temperature and may also be a factor contributing to high activities for materials prepared at higher temperatures. The specific surface areas for Ti-HTS-40, Ti-HTS-90, Ti-HTS-150, Ti-HTS-210, and Ti-HTS-240 are calculated to 24, 48, 98, 108, and 91 m^2/g, respectively. The enhanced activities for Ti-HTS-150, Ti-HTS-210, and Ti-HTS-240 may be attributed to their relatively high specific surface areas. In addition, a trend is observed between the rate of degradation and pore diameter of the materials. When the size of the pores increases, the rate of degradation may increase due to effective molecular transport. Thus, the presence of large pores favor enhanced diffusion of the dye molecules. Ti-HTS-40, Ti-HTS-90, Ti-HTS-150, Ti-HTS-210, and Ti-HTS-240 exhibit apparent degradation rate constants, (k_{app}) of 25.9×10^{-5}, 59.8×10^{-5}, 96.9×10^{-5}, 97.9×10^{-5}, and 109.8×10^{-5} s^{-1} having BJH pore diameters of 38, 66, 97, 123, and 175 Å, respectively. The pore volumes also

DOI: 10.1021/am508883f
ACS Appl. Mater. Interfaces 2015, 7, 4368−4380

Scheme 1. Possible Fragmented Primary Products of RhB Formed without Any Damage to the Ring Skeleton under Visible Light Irradiation

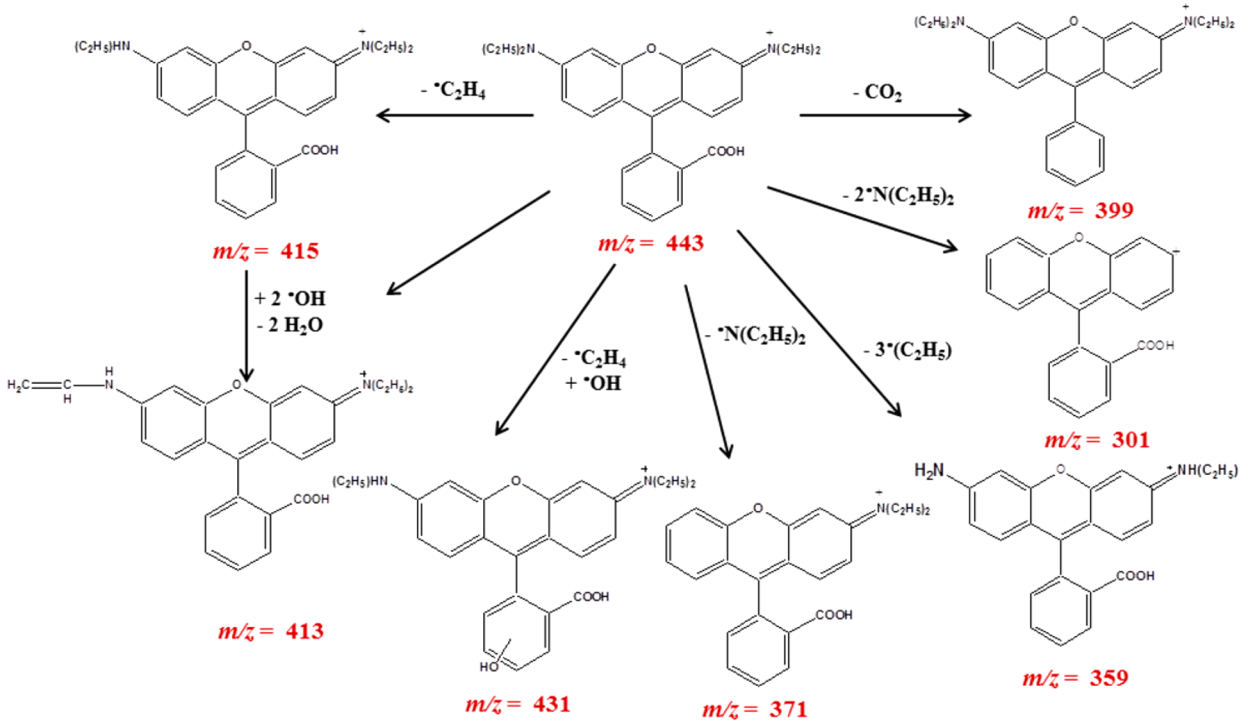

increase with increase in hydrothermal temperature suggesting it may also be a factor. Non-local density functional theory (NLDFT) analysis of the isotherms indicate absence of micropores. A plot (Figure 7) illustrates the correlation between the specific surface areas, percentages of surface hydroxyl groups, pore diameters of the material, and the degradation rate constants. The results suggest that an increase of hydrothermal temperatures, in general results in an increase in surface hydroxyl groups, specific surface areas, and porosity (pore diameters and pore volumes). Thus, the photocatalytic activities seem to be dependent on these three factors. In comparing the trends, we notice that the pore diameters increases with increase in hydrothermal treatment temperature, whereas the surface hydroxyl groups and specific surface areas seem to reach a plateau. This is perhaps indicative of the fact that the pore diameter has a pronounced effect in this study.

It has to be pointed out that we are comparing relative trends with a set of samples that only adsorbed a small amount <5% of RhB (Supporting Information Figure S7) prior to irradiation. Thus, the influence of RhB adsorption on the TiO_2 materials was found to be negligible in the degradation process and hence the apparent rate constants may be used as a guide to assess the photocatalytic activity.[64]

ESI-MS Analysis. The dye molecules degrade into several intermediates.[34,61] The degraded fragments formed during the visible light irradiation were evaluated by ESI-MS analysis over two selected samples, Ti-HTS-40 and Ti-HTS-240 that showed the lowest and highest activities, respectively. The fragmented molecular ions are detected in the acidic form (positive mode). It has been documented that the degradation of xanthene type dyes occurs via numerous steps[66−69] including, (i) *N*-de-ethylation/de-ethylation, (ii) dealkylation, (iii) deamination, (iv) decarboxylation, (v) dehydration, (vi) cleavage of chromophore or the destruction of the conjugation, and (vii) ring structure rupture. Under our experimental conditions, the mass spectrum of pure RhB dye solution, shows two major peaks at m/z = 443 and 413, which belongs to the parent dye molecule and the fragmented product with loss of water molecule after the de-ethylation of the dye molecule, respectively. Thus, an auto de-ethylation is possible for the RhB in solution under our MS experimental conditions. Even though both catalysts show similar fragmented peak profiles, the disappearance of the parent peak (m/z = 443) was achieved in a shorter time period with the catalyst Ti-HTS-240 than Ti-HTS-40 because of its high activity (Figure 8).

In addition, the intensity (counts) of the parent peak at m/z = 443 decreases with time suggesting its degradation. The peaks at m/z = 443, 431, 415, 413, 371, 359, and 301 correspond to degradation products, which are formed without any damage to the ring skeleton of the RhB molecule as indicated in Scheme 1.

The de-ethylation of the parent compound followed by an addition of −OH group results in a peak at m/z = 431, whereas de-ethylation alone results in a peak at m/z = 415. Attack of •OH, to the de-ethylated molecule (m/z = 415) initiates the elimination of two water molecules and results in a peak at m/z = 413. Although the above-mentioned peaks were obtained with the two selected catalysts Ti-HTS-40 and Ti-HTS-240, the peak at m/z = 371 was obtained only with Ti-HTS-40 catalyst after 180 min of visible irradiation due to the *N*-de-ethylation (loss of $\bullet N(C_2H_5)_2$) from RhB molecule. This may be due to the slower degradation rate of Ti-HTS-40, which allows for the formation of this fragment after a longer time of irradiation (180 min). The removal of three moles of ethyl groups from the parent molecule results in a peak at m/z = 359, after 90 min of irradiation with Ti-HTS-40. However, the same peak was observed after only 15 min of irradiation with Ti-HTS-240. A peak at m/z = 301 was obtained in both the samples at different irradiation times because of the complete *N*-de-ethylation (of two moles of $\bullet N(C_2H_5)_2$) from the parent RhB molecule. In

DOI: 10.1021/am508883f
ACS Appl. Mater. Interfaces 2015, 7, 4368−4380

Scheme 2. Plausible Fragments of RhB after the Cleavage of Carbon−Oxygen Bond in the RhB Ring Structure, under Visible Light Irradiation

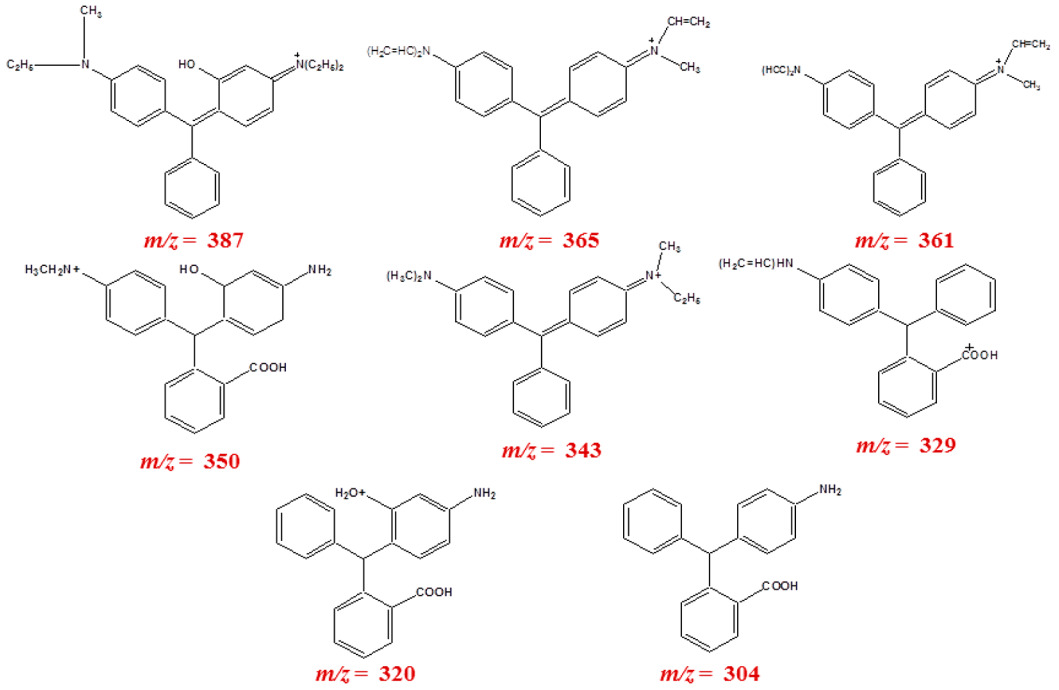

addition, a peak at m/z = 399 was observed with Ti-HTS-240 material only after 60 min of irradiation in this study.

The peaks at m/z = 387, 365, 361, 350, 343, 329, 320, and 304 were observed after the cleavage of carbon−oxygen bond in the ring structure as illustrated in Scheme 2.

In particular, the peaks at m/z = 329, 320, and 304 appeared only with the catalyst Ti-HTS-240 after 45 min of visible light irradiation. This may be due to the larger pore size of this sample that is able to accommodate the RhB fragmented products inside the pores for a reasonable amount of time and then allow them for further stepwise fragmentation. The peaks at m/z = 313, 283, 249, and 210 were obtained after the cleavage of one ring structure from the secondary fragments, and the peak at m/z = 210 was observed only with the catalyst Ti-HTS-240 after 45 min of irradiation as explained in Scheme 3.

The chromophore cleavage from secondary fragmented products of RhB molecules results in the formation of molecules with one benzene ring structure, which generates peaks at m/z = 194, 192, 167, 150, 149, 136, 109, and 95. The molecular ion structures of these secondary fragmented products are illustrated in Scheme 4A. Finally, the ring opening results in peaks at m/z = 114, 87, 83, 74, 71, and 69 and these peaks were observed with both the catalysts (Scheme 4B).

All the ESI-MS spectra obtained at different time intervals with the two selected photocatalysts along with the MS of pure RhB are shown in the Supporting Information, Figures S8 to S22.

Additional experiments were carried out with different scavenging agents to further understand the role of O_2, and hydroxyl radicals ($^{\bullet}OH$).

Scheme 3. Possible Fragments of RhB after the Cleavage of One Benzene Ring from the Fragmented RhB Molecule, under Visible Light Irradiation

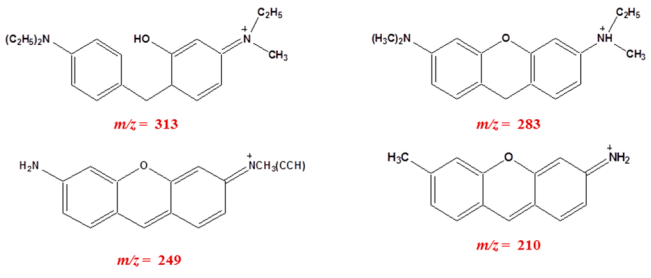

Photocatalysis in the Presence of Scavenging Agents. The differences in the dye removal efficiencies in the presence of different scavenging agents were investigated with the material Ti-HTS-240, which showed the highest activity in this study. The role of molecular O_2 was tested by carrying out the experiments under N_2 flow. The absorbance spectrum (Supporting Information Figure S23) shows no shift in the peaks at λ_{max} = 554 and λ_{max} = 258 nm indicating that the dye molecules are not degraded and that the conjugated structure of the dye molecules is retained throughout the course of experiment.[70] This validates the importance of dissolved oxygen for the degradation process [eq 3]. The electrons, which are injected from the excited dye molecules to the conduction band of the semiconductor materials during the irradiation, react with oxygen and form superoxide ($O_2^{\bullet-}$) radicals that assist in the degradation of dye in the presence of photocatalyst (TiO_2). The superoxide radical further provides the necessary ROS for the degradation process explained in the eqs 4−7. The inert atmosphere (N_2 flow) inhibits the formation of the above-mentioned ROS species and this prevents degradation of RhB.

Isopropyl alcohol, a hydroxyl radical ($^{\bullet}OH$) trapping agent, was utilized in the degradation process to provide more insight about the role of $^{\bullet}OH$ radical in the dye degradation process. Once again we noticed no shifts in peaks at λ_{max} = 554 and 258 nm indicating that RhB is not degraded (Supporting

DOI: 10.1021/am508883f
ACS Appl. Mater. Interfaces 2015, 7, 4368−4380

Scheme 4. Possible Fragments of RhB after (A) Cleavage of Chromophore and (B) Ring Opening under Visible Light Irradiation

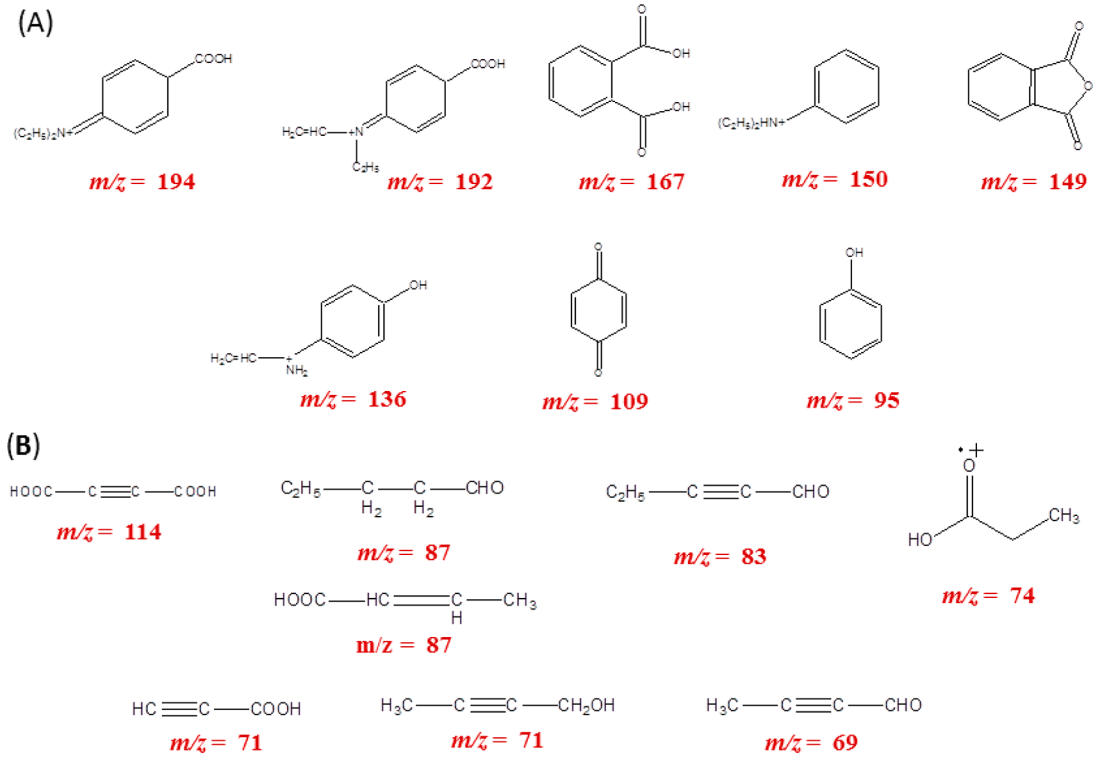

Information Figure S24). This suggests that hydroxyl radicals are scavenged by IPA [eq 8].

$$HO^{\bullet} + HC(CH_3)_2OH \rightarrow {}^{\bullet}C(CH_3)_2OH + H_2O \quad (8)$$

It is known that hydroxyl radicals play an important role in the dye degradation. To shed more light on this, $^{\bullet}$OH trapping experiments were carried out. These radicals can react with terephthalic acid (TPA) and form fluorescent 2-hydroxyterephthalic acid (2-HTPA). The formation of 2-HTPA is proportional to the amount of $^{\bullet}$OH formed. Figure 9 shows a plot of fluorescence intensity for 2-HTPA versus time for all the catalysts used in this study.

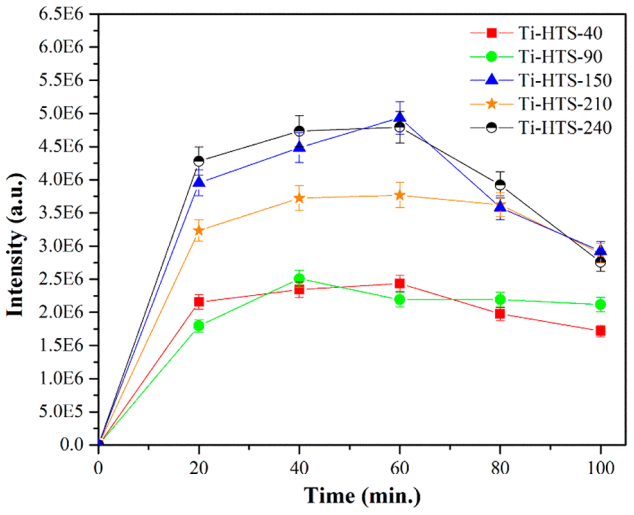

Figure 9. Plot of fluorescence intensity of 2-HTPA vs time for TiO_2 materials.

It can be seen from Figure 9 that the production of $^{\bullet}$OH radical in the samples Ti-HTS-40 and Ti-HTS-90 are relatively small in comparison to other three catalysts, and, thus, these two materials shows <90% dye removal (i.e., 57% and 88% dye removal, respectively) after 180 min of time period, while the other three materials (Ti-HTS-150, Ti-HTS-210, and Ti-HTS-240) shows almost complete dye removal (>97%) in the same duration. Thus, $^{\bullet}$OH radicals play an important role in the photocatalytic degradation. The results obtained from our scavenging experiments suggest that the degradation of RhB was highly affected by the hydroxyl and superoxide radicals.

CONCLUSIONS

A set of TiO_2 materials were successfully prepared with different pore sizes by simply varying the hydrothermal treatment temperature without the need for surfactants, auxiliary chemicals, structure directing agents, or supercritical conditions. RhB degradation was examined using TiO_2 materials under visible light irradiation, and it was found that the rate of degradation is dependent on the pore sizes, specific surface areas, and surface hydroxyl groups of the materials. Larger pore sized materials favor effective diffusion of RhB molecules to the active sites of the TiO_2 resulting in enhanced degradation. The results from ESI-MS studies provide detailed information regarding the nature of degraded products at different time intervals. Superoxide and hydroxyl radicals seem to be important for the dye degradation. This work provides a new, simple, and effective method to tune the porosity and enhance the photocatalytic activities of titanium dioxide based materials.

DOI: 10.1021/am508883f
ACS Appl. Mater. Interfaces 2015, 7, 4368−4380

■ ASSOCIATED CONTENT

Supporting Information

Tables for optimal conditions for ESI-MS studies, rate constants for dye degradation, characterization (Raman, FT-IR, TGA, TEM, and SEM), UV−vis absorption spectra of RhB (after dye degradation and after dye adsorption), ESI-MS of RhB solution after photocatalytic degradation at various intervals of irradiation (15, 30, 45, 60, etc.), and UV−vis absorption spectra of RhB from scavenging experiments. This material is available free of charge via the Internet at http://pubs.acs.org.

■ AUTHOR INFORMATION

Corresponding Author

*Tel: 605-677-6189. Fax: 605-677-6397. E-mail: Ranjit.Koodali@usd.edu.

Notes

The authors declare no competing financial interest.

■ ACKNOWLEDGMENTS

We extend sincere gratitude to NSF-CHE-0619190, NSF-CHE-0722632, NSF-EPS-0903804, DE-EE0000270, NNX12AB17G, and SD-BoR for funding this project. Thanks are due to Eric Harmon for SEM measurements.

■ REFERENCES

(1) Lachheb, H.; Puzenat, E.; Houas, A.; Ksibi, M.; Elaloui, E.; Guillard, C.; Herrmann, J.-M. Photocatalytic Degradation of Various Types of Dyes (Alizarin S, Crocein Orange G, Methyl Red, Congo Red, Methylene Blue) in Water by UV-Irradiated Titania. *Appl. Catal., B* **2002**, *39*, 75−90.

(2) Aboul-Gheit, A.; Abdel-Hamid, S.; Mahmoud, S.; El-Salamony, R.; Valyon, J.; Mihályi, M.; Szegedi, Á. Mesoporous Ti-MCM-41 Materials as Photodegradation Catalysts of 2,4,6-Trichlorophenol in Water. *J. Mater. Sci.* **2011**, *46*, 3319−3329.

(3) Guillard, C.; Disdier, J.; Monnet, C.; Dussaud, J.; Malato, S.; Blanco, J.; Maldonado, M. I.; Herrmann, J.-M. Solar Efficiency of A New Deposited Titania Photocatalyst: Chlorophenol, Pesticide, and Dye Removal Applications. *Appl. Catal., B* **2003**, *46*, 319−332.

(4) Sud, D.; Kaur, P. Heterogeneous Photocatalytic Degradation of Selected Organophosphate Pesticides: A Review. *Crit. Rev. Environ. Sci. Technol.* **2011**, *42*, 2365−2407.

(5) Xu, Y.; Lebrun, R. E.; Gallo, P.-J.; Blond, P. Treatment of Textile Dye Plant Effluent by Nanofiltration Membrane. *Sep. Sci. Technol.* **1999**, *34*, 2501−2519.

(6) Won, S. W.; Choi, S. B.; Chung, B. W.; Park, D.; Park, J. M.; Yun, Y. S. Biosorptive Decolorization of Reactive Orange 16 Using the Waste Biomass of Corynebacterium Glutamicum. *Ind. Eng. Chem. Res.* **2004**, *43*, 7865−7869.

(7) Pelegrini, R.; Peralta-Zamora, P.; de Andrade, A. R.; Reyes, J.; Durán, N. Electrochemically Assisted Photocatalytic Degradation of Reactive Dyes. *Appl. Catal., B* **1999**, *22*, 83−90.

(8) Chatterjee, S.; Chatterjee, S.; Chatterjee, B. P.; Das, A. R.; Guha, A. K. Adsorption of a Model Anionic Dye, Eosin Y, from Aqueous Solution by Chitosan Hydrobeads. *J. Colloid Interface Sci.* **2005**, *288*, 30−35.

(9) Dong, Y. L.; Lu, B.; Zang, S. Y.; Zhao, J. X.; Wang, X. G.; Cai, Q. H. Removal of Methylene Blue from Coloured Effluents by Adsorption onto SBA-15. *J. Chem. Technol. Biotechnol.* **2011**, *86*, 616−619.

(10) Messina, P. V.; Schulz, P. C. Adsorption of Reactive Dyes on Titania−Silica Mesoporous Materials. *J. Colloid Interface Sci.* **2006**, *299*, 305−320.

(11) Ahmad, R.; Mondal, P. K.; Usmani, S. Q. Hybrid UASFB-Aerobic Bioreactor for Biodegradation of Acid Yellow-36 in Wastewater. *Bioresour. Technol.* **2010**, *101*, 3787−3790.

(12) Guo, W.; Liu, X.; Huo, P.; Gao, X.; Wu, D.; Lu, Z.; Yan, Y. Hydrothermal Synthesis Spherical TiO_2 and Its Photo-Degradation Property on Salicylic Acid. *Appl. Surf. Sci.* **2012**, *258*, 6891−6896.

(13) Guo, Y.; Yang, S.; Zhou, X.; Lin, C.; Wang, Y.; Zhang, W. Enhanced Photocatalytic Activity for Degradation of Methyl Orange over Silica-Titania. *J. Nanomater.* **2011**, No. 296953.

(14) He, Z.; Sun, C.; Yang, S.; Ding, Y.; He, H.; Wang, Z. Photocatalytic Degradation of Rhodamine B by Bi_2WO_6 With Electron Accepting Agent Under Microwave Irradiation: Mechanism and Pathway. *J. Hazard. Mater.* **2009**, *162*, 1477−1486.

(15) Kuang, L. Y.; Zhao, Y. P.; Liu, L. Photodegradation of Orange II by Mesoporous TiO_2. *J. Environ. Monitor.* **2011**, *13*, 2496−2501.

(16) Li, J.; Chen, C.; Zhao, J.; Zhu, H.; Orthman, J. Photodegradation of Dye Pollutants on TiO_2 Nanoparticles Dispersed in Silicate Under UV−Vis Irradiation. *Appl. Catal., B* **2002**, *37*, 331−338.

(17) Li, J.; Ma, W.; Chen, C.; Zhao, J.; Zhu, H.; Gao, X. Photodegradation of Dye Pollutants on One-Dimensional TiO_2 Nanoparticles Under UV and Visible Irradiation. *J. Mol. Catal. A: Chem.* **2007**, *261*, 131−138.

(18) Vohra, M. S.; Tanaka, K. Photocatalytic Degradation of Aqueous Pollutants Using Silica-Modified TiO_2. *Water Res.* **2003**, *37*, 3992−3996.

(19) Konsowa, A. H.; Ossman, M. E.; Chen, Y.; Crittenden, J. C. Decolorization of Industrial Wastewater by Ozonation Followed by Adsorption on Activated Carbon. *J. Hazard. Mater.* **2010**, *176*, 181−185.

(20) Chong, M. N.; Jin, B.; Chow, C. W. K.; Saint, C. Recent Developments in Photocatalytic Water Treatment Technology: A Review. *Water Res.* **2010**, *44*, 2997−3027.

(21) Comninellis, C.; Kapalka, A.; Malato, S.; Parsons, S. A.; Poulios, I.; Mantzavinos, D. Advanced Oxidation Processes for Water Treatment: Advances and Trends for R&D. *J. Chem. Technol. Biotechnol.* **2008**, *83*, 769−776.

(22) Atul, V. W.; Gaikwad, G. S.; Dhonde, M. G.; Khaty, N. T.; Thakare, S. R. Removal of Organic Pollutant from Water by Heterogenous Photocatalysis: A Review. *Res. J. Chem. Environ.* **2013**, *17*, 84−94.

(23) Choi, W. Pure and Modified TiO_2 Photocatalysts and Their Environmental Applications. *Catal. Surv. Asia* **2006**, *10*, 16−28.

(24) Hoffmann, M. R.; Martin, S. T.; Choi, W.; Bahnemann, D. W. Environmental Applications of Semiconductor Photocatalysis. *Chem. Rev.* **1995**, *95*, 69−96.

(25) Pelaez, M.; Nolan, N. T.; Pillai, S. C.; Seery, M. K.; Falaras, P.; Kontos, A. G.; Dunlop, P. S. M.; Hamilton, J. W. J.; Byrne, J. A.; O'Shea, K.; Entezari, M. H.; Dionysiou, D. D. A Review on the Visible Light Active Titanium Dioxide Photocatalysts for Environmental Applications. *Appl. Catal., B* **2012**, *125*, 331−349.

(26) Doll, T. E.; Frimmel, F. H. Removal of Selected Persistent Organic Pollutants by Heterogeneous Photocatalysis in Water. *Catal. Today* **2005**, *101*, 195−202.

(27) Gaya, U. I.; Abdullah, A. H. Heterogeneous Photocatalytic Degradation of Organic Contaminants over Titanium Dioxide: A Review of Fundamentals, Progress, and Problems. *J. Photochem. Photobiol., C* **2008**, *9*, 1−12.

(28) Herrmann, J.-M. Heterogeneous Photocatalysis: Fundamentals and Applications to the Removal of Various Types of Aqueous Pollutants. *Catal. Today* **1999**, *53*, 115−129.

(29) Yin, M.; Li, Z.; Kou, J.; Zou, Z. Mechanism Investigation of Visible Light-Induced Degradation in a Heterogeneous TiO_2/Eosin Y/Rhodamine B System. *Environ. Sci. Technol.* **2009**, *43*, 8361−8366.

(30) Gude, K.; Gun'ko, V. M.; Blitz, J. P. Adsorption and Photocatalytic Decomposition of Methylene Blue on Surface Modified Silica and Silica-Titania. *Colloids Surf., A* **2008**, *325*, 17−20.

(31) Zanjanchi, M. A.; Sajjadi, H.; Arvand, M.; Mohammad-Khah, A.; Ghalami-Choobar, B. Modification of MCM-41 with Anionic Surfactant: A Convenient Design for Efficient Removal of Cationic Dyes from Wastewater. *Clean: Soil, Air, Water* **2011**, *39*, 1007−1013.

(32) Zakaria, M. B.; Suzuki, N.; Shimasaki, K.; Miyamoto, N.; Huang, Y. T.; Yamauchi, Y. Synthesis of Mesoporous Titania Nanoparticles

DOI: 10.1021/am508883f
ACS Appl. Mater. Interfaces 2015, 7, 4368−4380

with Anatase Frameworks and Investigation of Their Photocatalytic Performance. *J. Nanosci. Nanotechnol.* **2012**, *12*, 4502−4507.
(33) Thapa, R.; Maiti, S.; Rana, T. H.; Maiti, U. N.; Chattopadhyay, K. K. Anatase TiO_2 Nanoparticles Synthesis via Simple Hydrothermal Route: Degradation of Orange II, Methyl Orange and Rhodamine B. *J. Mol. Catal. A: Chem.* **2012**, *363*, 223−229.
(34) Li, J.-Y.; Ma, W.-H.; Lei, P.-X.; Zhao, J.-C. Detection of Intermediates in the TiO_2-Assisted Photodegradation of Rhodamine B Under Visible Light Irradiation. *J. Environ. Sci.* **2007**, *19*, 892−896.
(35) Li, W.; Li, D.; Meng, S.; Chen, W.; Fu, X.; Shao, Y. Novel Approach to Enhance Photosensitized Degradation of Rhodamine B Under Visible Light Irradiation by the $Zn_xCd_{1-x}S/TiO_2$ Nanocomposites. *Environ. Sci. Technol.* **2011**, *45*, 2987−2993.
(36) Liu, K.; Zhu, L.; Li, N.; Sun, Y.; Li, H.; Zhu, X. Solvothermal Synthesis of Mesoporous Slabstone-Like TiO_2 and Its Photodegradation Preference in A Methyl Orange-Rhodamine B Mixture Solution. *Crys. Res. Technol.* **2012**, *47*, 1088−1094.
(37) Pang, Y. L.; Abdullah, A. Z. Effect of Carbon and Nitrogen Co-Doping on Characteristics and Sonocatalytic Activity of TiO_2 Nanotubes Catalyst for Degradation of Rhodamine B in Water. *Chem. Eng. J.* **2013**, *214*, 129−138.
(38) Sayilkan, F.; Asilturk, M.; Sener, S.; Erdemoglu, S.; Erdemoglu, M.; Sayilkan, H. Hydrothermal Synthesis, Characterization, and Photocatalytic Activity of Nanosized TiO_2 Based Catalysts for Rhodamine B Degradation. *Turk. J. Chem.* **2007**, *31*, 211−221.
(39) Shi, X. L.; Yang, X. Y.; Wang, S. W.; Wang, S.; Zhang, Q. X.; Wang, Y. F. Photocatalytic Degradation of Rhodamine B Dye with High Purity Anatase Nano-TiO_2 Synthesized by A Hydrothermal Method. *J. Wuhan Univ. Technol.* **2011**, *26*, 600−605.
(40) Wilhelm, P.; Stephan, D. Photodegradation of Rhodamine B in Aqueous Solution via SiO_2@TiO_2 Nano-Spheres. *J. Photochem. Photobiol., A* **2007**, *185*, 19−25.
(41) Grabowska, E.; Reszczyńska, J.; Zaleska, A. Mechanism of Phenol Photodegradation in the Presence of Pure and Modified-TiO_2: A Review. *Water Res.* **2012**, *46*, 5453−5471.
(42) Tian, L.; Liu, H.; Gao, Y. Degradation and Adsorption of Rhodamine B and Phenol on TiO_2/MCM-41. *Kinet. Catal.* **2012**, *53*, 554−559.
(43) Ilisz, I.; Dombi, A.; Mogyorósi, K.; Farkas, A.; Dékány, I. Removal of 2-Chlorophenol from Water by Adsorption Combined with TiO_2 Photocatalysis. *Appl. Catal., B* **2002**, *39*, 247−256.
(44) Juang, L. C.; Semblante, G. U.; You, S. J.; Hong, S. H. Degradation of 2-Chlorophenol Using Carbon Nanotube/Titanium Oxide Composite Prepared by Hydrothermal Method. *J. Taiwan Inst. Chem. Eng.* **2013**, *44*, 432−437.
(45) Wang, K.-H.; Hsieh, Y.-H.; Chou, M.-Y.; Chang, C.-Y. Photocatalytic Degradation of 2-Chloro and 2-Nitrophenol by Titanium Dioxide Suspensions in Aqueous Solution. *Appl. Catal., B* **1999**, *21*, 1−8.
(46) Luo, H. Y.; Nie, X.; Li, G. Y.; Liu, J. K.; An, T. C. Structural Characterization and Photocatalytic Activity of Hydrothermally Synthesized Mesoporous TiO_2 for 2,4,6-Tribromophenol Degradation in Water. *Chin. J. Catal.* **2011**, *32*, 1349−1356.
(47) Melian, E. P.; Diaz, O. G.; Rodriguez, J. M. D.; Colon, G.; Navio, J. A.; Pena, J. P. Effect of Hydrothermal Treatment on Structural and Photocatalytic Properties of TiO_2 Synthesized by Sol−Gel Method. *Appl. Catal., A* **2012**, *411*, 153−159.
(48) Zhang, X. M.; Huo, K. F.; Wang, H. R.; Zhang, W. R.; Chu, P. K. Influence of Structure Parameters and Crystalline Phase on the Photocatalytic Activity of TiO_2 Nanotube Arrays. *J. Nanosci. Nanotechnol.* **2011**, *11*, 11200−11205.
(49) Dong, W.; Lee, C. W.; Lu, X.; Sun, Y.; Hua, W.; Zhuang, G.; Zhang, S.; Chen, J.; Hou, H.; Zhao, D. Synchronous Role of Coupled Adsorption and Photocatalytic Oxidation on Ordered Mesoporous Anatase TiO_2−SiO_2 Nanocomposites Generating Excellent Degradation Rctivity of RhB Dye. *Appl. Catal., B* **2010**, *95*, 197−207.
(50) Roca, R. A.; Leite, E. R. Size and Shape Tailoring of Titania Nanoparticles Synthesized by Solvothermal Route in Different Solvents. *J. Am. Ceram. Soc.* **2013**, *96*, 96−102.
(51) Chen, W.; Qiu, Y.; Yan, K.; Yang, S. Surfactant Directed Self-Assembly of Size-Tunable Mesoporous Titanium Dioxide Microspheres and Their Application in Quasi-Solid State Dye-Sensitized Solar Cells. *J. Power Sources* **2011**, *196*, 10806−10816.
(52) Sreethawong, T.; Ngamsinlapasathian, S.; Yoshikawa, S. Influences of Urea−Glycerol Mixtures as Mixed Mesopore-Controlling Agents on Tailoring Physicochemical Properties and Photocatalytic H_2 Production Activity of Sol−Gel Derived Mesoporous Assembled TiO_2 Nanocrystals. *Mater. Res. Bull.* **2013**, *48*, 30−36.
(53) Zhang, Y.; Zhang, S.; Wang, K.; Ding, F.; Wu, J. Surfactant-Free Solvothermal Method for Synthesis of Mesoporous Nanocrystalline TiO_2 Microspheres with Tailored Pore Size. *J. Nanomater.* **2013**, *2013*, 7.
(54) Yu, J.; Yu, J. C.; Ho, W.; Leung, M. K. P.; Cheng, B.; Zhang, G.; Zhao, X. Effects of Alcohol Content and Calcination Temperature on the Textural Properties of Bimodally Mesoporous Titania. *Appl. Catal., A* **2003**, *255*, 309−320.
(55) Sreethawong, T.; Suzuki, Y.; Yoshikawa, S. Photocatalytic Evolution of Hydrogen Over Nanocrystalline Mesoporous Titania Prepared by Surfactant-Assisted Templating Sol−Gel Process. *Catal. Commun.* **2005**, *6*, 119−124.
(56) Capello, C.; Fischer, U.; Hungerbuhler, K. What is a Green Solvent? A Comprehensive Framework for the Environmental Assessment of Solvents. *Green Chem.* **2007**, *9*, 927−934.
(57) Meador, M. A. B.; Weber, A. S.; Hindi, A.; Naumenko, M.; McCorkle, L.; Quade, D.; Vivod, S. L.; Gould, G. L.; White, S.; Deshpande, K. Structure−Property Relationships in Porous 3D Nanostructures: Epoxy-Cross-Linked Silica Aerogels Produced Using Ethanol as the Solvent. *ACS Appl. Mater. Interfaces* **2009**, *1*, 894−906.
(58) Wu, Q. L.; Rankin, S. E. Tuning the Mesopore Size of Titania Thin Films Using a Polymeric Swelling Agent. *J. Phys. Chem. C* **2011**, *115*, 11925−11933.
(59) Leite Vasconcelos, D. C.; Costa, V. C.; Martins Nunes, E. H.; Soares Sabioni, A. C.; Gasparon, M.; Vasconcelos, W. L. Infrared Spectroscopy of Titania Sol−Gel Coatings on 316L Stainless Steel. *Mater. Sci. Appl.* **2011**, *2*, 1375−1382.
(60) Hayashi, H.; Torii, K. Hydrothermal Synthesis of Titania Photocatalyst under Subcritical and Supercritical Water Conditions. *J. Mater. Chem.* **2002**, *12*, 3671−3676.
(61) Chen, F.; Zhao, J.; Hidaka, H. Highly Selective Deethylation of Rhodamine B: Adsorption and Photooxidation Pathways of the Dye on the TiO_2/SiO_2 Composite Photocatalyst. *Int. J. Photoenergy* **2003**, *5*, 209−217.
(62) Akpan, U. G.; Hameed, B. H. Parameters Affecting the Photocatalytic Degradation of Dyes Using TiO_2-Based Photocatalysts: A Review. *J. Hazard. Mater.* **2009**, *170*, 520−529.
(63) Wu, T.; Liu, G.; Zhao, J.; Hidaka, H.; Serpone, N. Photoassisted Degradation of Dye Pollutants. V. Self-Photosensitized Oxidative Transformation of Rhodamine B Under Visible Light Irradiation in Aqueous TiO_2 Dispersions. *J. Phys. Chem. B* **1998**, *102*, 5845−5851.
(64) Rasalingam, S.; Kibombo, H. S.; Wu, C. M.; Budhi, S.; Peng, R.; Baltrusaitis, J.; Koodali, R. T. Influence of Ti−O−Si Hetero-Linkages in the Photocatalytic Degradation of Rhodamine B. *Catal. Commun.* **2013**, *31*, 66−70.
(65) Xu, Y.; Langford, C. H. UV- or Visible-Light-Induced Degradation of X3B on TiO_2 Nanoparticles:The Influence of Adsorption. *Langmuir* **2001**, *17*, 897−902.
(66) Yang, Y.; Guo, Y.; Hu, C.; Jiang, C.; Wang, E. Synergistic Effect of Keggin-Type $[X^{n+}W_{11}O_{39}]^{(12-n)-}$ and TiO_2 in Macroporous Hybrid Materials $[X^{n+}W_{11}O_{39}]^{(12-n)-}TiO_2$ for the Photocatalytic Degradation of Textile Dyes. *J. Mater. Chem.* **2003**, *13*, 1686−1694.
(67) He, Z.; Yang, S.; Ju, Y.; Sun, C. Microwave Photocatalytic Degradation of Rhodamine B Using TiO_2 Supported on Activated Carbon: Mechanism Implication. *J. Environ. Sci.* **2009**, *21*, 268−272.
(68) Martínez-de la Cruz, A.; Pérez, U. M. G. Photocatalytic Properties of $BiVO_4$ Prepared by the Co-Precipitation Method: Degradation of Rhodamine B and Possible Reaction Mechanisms Under Visible Irradiation. *Mater. Res. Bull.* **2010**, *45*, 135−141.

DOI: 10.1021/am508883f
ACS Appl. Mater. Interfaces 2015, 7, 4368−4380

(69) Chen, C.; Lu, C. Photocatalytic Degradation of Basic Violet 4: Degradation Efficiency, Product Distribution, and Mechanisms. *J. Phys. Chem. C* **2007**, *111*, 13922−13932.
(70) Horikoshi, S.; Hidaka, H.; Serpone, N. Environmental Remediation by An Integrated Microwave/UV-Illumination Method. 1. Microwave-Assisted Degradation of Rhodamine-B Dye in Aqueous TiO_2 Dispersions. *Environ. Sci. Technol.* **2002**, *36*, 1357−1366.

DOI: 10.1021/am508883f
ACS Appl. Mater. Interfaces 2015, 7, 4368−4380